A computational model for cell morphodynamics

Danying Shao, **Wouter-Jan Rappel**, and **Herbert Levine**
Center for Theoretical Biological Physics and Department of Physics, University of California, San Diego, La Jolla, CA 92093-0374, USA

Abstract

We develop a computational model, based on the phase field method, for cell morphodynamics and apply it to fish keratocytes. Our model incorporates the membrane bending force and the surface tension and enforces a constant area. Furthermore, it implements a cross linked actin filament field and an actin bundle field that are responsible for the protrusion and retraction forces, respectively. We show that our model predicts steady state cell shapes with a wide range of aspect ratios, depending on system parameters. Furthermore, we find that the dependence of the cell speed on this aspect ratio matches experimentally observed data.

Many eukaryotic cells can move using a crawling motion during which the front of the cell is extended by the polymerization of an actin filaments network. Forces applied to the substrate are mediated through adhesion and the detachment of the back of the cell is regulated by myosin and other proteins [1]. The modeling of this type of cell movement is a complex undertaking for several different reasons. First of all, the underlying signaling pathways responsible for controlling the movement are often poorly understood. For example, in eukaryotic chemotaxis, where cells are guided by chemical gradients, it is still unclear how cells determine their direction [2]. Furthermore, the forces that are generated during cell motion are most often not quantified, although recent experiments have started to address the cell-substrate interaction [3]. Lastly, cell movement is a dynamic process, involving cell membrane deformations and retractions that require a computational modeling strategy that can handle deformable boundaries. Not surprisingly, only a limited number of studies have attempted to address morphodynamics, the cell shape dynamics during movement (for a review, see [1]).

In this paper, we construct a quantitative model for cell shape dynamics during motion based on the phase-field method [4,5]. This method introduces an auxiliary field that distinguishes the interior of the cell from the exterior. The dynamics of the cell is governed by equations that couple this field to the actual physical degrees of freedom, and the diffuse layer separating the interior from the exterior marks the membrane location. Importantly, this technique does not require the explicit tracking of this boundary. The phase-field method has been successfully applied to wide ranging problems such as solidification [6], crack propagation [7], viscous fingering [8] and diffusional problems in complicated geometries [9,10]. To develop our method, we apply it to the specific case of the motion of epithelial keratocytes. These cells extend a thin lamellipodium at the front and sides, with a bulbous cell body attached at the back [12]. Importantly, these cells can maintain rapid and persistent gliding motion over several cell lengths in the absence of external stimuli[13–15].

We model the keratocyte as a two dimensional sheet with a fixed area A_0, although the extension to three dimensions is straightforward (albeit computationally expensive). The phase field takes on $\varphi = 1$ in the interior of the cell and $\varphi = 0$ represents the cell exterior. The shape of the cell membrane is determined by the interactions of various forces, including the surface tension, the bending force and the pressure that constrains the cell area, as in vesicles. We do not fix the cell perimeter, allowing the amount of membrane to change due

to either the smoothing out of small-scale wrinkles or due to endo/exocytosis. We also consider the protrusion force from cross-linked actin filaments, the contraction force from the actin bundles and the effective friction due to cells' adhesion and attachment/detachment from the substrates.

The surface energy is proportional to the cell's perimeter L and can be implemented in the phase field formulations as [16,18]

$$\mathcal{H}_{\text{ten}}=\gamma L=\gamma \int \left(\frac{\epsilon}{2}|\nabla\phi|^2+\frac{G}{\epsilon} \right) d\mathbf{r},$$

where γ is the surface tension, ε is the parameter controlling the width of the cell boundary and where $G(\varphi) = 18\varphi^2(1 - \varphi)^2$ is a double well potential with minima at $\varphi = 0$ and $\varphi = 1$. The area density of surface tension force is derived as follows:

$$\mathbf{F}_{\text{ten}}^{*}= - \frac{\delta\mathcal{H}_{\text{ten}}}{\delta\mathbf{R}}=\frac{\delta\mathcal{H}_{\text{ten}}}{\delta\phi}\nabla\phi= - \gamma \left(\epsilon\nabla^2\phi - \frac{G'}{\epsilon} \right)\nabla\phi$$

This area density can be converted into a line density using $\mathbf{F}_{\text{ten}}^{*}d\mathbf{r}=\mathbf{F}_{\text{ten}}dl=F_{\text{ten}} \, \epsilon \, |\nabla\phi|^2 d\mathbf{r}$. Thus

$$\mathbf{F}_{\text{ten}}= - \gamma \left(\nabla^2\phi - \frac{G'}{\epsilon^2} \right) \frac{\nabla\phi}{|\nabla\phi|^2}.$$

This can also be seen by noting that the expression in brackets will vanish identically for thin planar interfaces if the phase field free energy $\mathcal{F}[\phi] = \int \frac{1}{\epsilon}\left[\frac{(\epsilon|\nabla\phi|)^2}{2}+G \right]\mathbf{r}$ is minimized, and hence picks up its leading term from considering the expansion for a slightly curved thin interface with normal $\widehat{n}$ and curvature c: $\nabla^2\phi \simeq (\widehat{n} \cdot \nabla)^2\phi+c\widehat{n} \cdot \nabla\phi$. Therefore, the tension force follows $\mathbf{F}_{\text{ten}}= - \gamma c\widehat{n}$. This is consistent with the Young-Laplace equation, which states that the net component of the surface tension forces is normal to the surface and proportional to the local curvature.

Helfrich [21] modeled the bending energy as $\mathcal{H}_{\text{bend}}=\frac{\kappa}{2} \oint c^2 dl$ where κ is the bending rigidity and where l denotes the arclength along the perimeter. This term can be implemented as [16,18]

$$\mathcal{H}_{\text{bend}}=\frac{\kappa}{2} \int \frac{1}{\epsilon}\left[\epsilon\nabla^2\phi - \frac{1}{\epsilon}G' \right]^2 d\mathbf{r}$$

Note that we have taken the spontaneous curvature to be 0. We then derive the bending force's area density and convert it into a line density as above:

$$\mathbf{F}_{\text{bend}}=\kappa \left(\nabla^2 - \frac{G''}{\epsilon^2} \right)\left(\nabla^2\phi - \frac{G'}{\epsilon^2} \right) \frac{\nabla\phi}{|\nabla\phi|^2}$$

We have verified that this expression is identical to the one employed by Biben and Misbah [19].

Experiments show that the cell area $A = \int \varphi r$ is conserved during deformation and movement [12]; the same study indicates that perimeter is not highly conserved. Thus we introduce a constraint term:

$$\mathbf{F}_{\text{area}} = -M_A (A - A_0)\widehat{n} = M_A \left(\int \phi d\mathbf{r} - A_0\right) \frac{\nabla\phi}{|\nabla\phi|}$$

where M_A is large and where A_0 is the prescribed area.

The coupling of the actin-myosin system provides a differential extension/retraction force for the cell membrane and thus generates the cell's movement. Specifically, at the leading edge of the cell, the actin filaments form a highly cross-linked network and the polymerization of actin filaments pushes the cell membrane forward. At the back of the cell actin filaments reorganize and align into bundles which, with the help of the molecular motor myosin-II, generate retraction forces [22,23]. Despite intensive studies on the actin-myosin system, the detailed mechanisms underlying this system are still quantitatively uncertain. We will therefore proceed phenomenologically and assume that the protrusion and retraction force is simply proportional to the concentration of cross-linked actin filaments, denoted by V, and the concentration of actin bundles, denoted by W:

$$\mathbf{F}_{\text{prot}} = \alpha V\widehat{n} = -\alpha V \frac{\nabla\phi}{|\nabla\phi|}; \mathbf{F}_{retr} = -\beta W\widehat{n} = \beta W \frac{\nabla\phi}{|\nabla\phi|}$$

where α and β are coefficients that determine the magnitude of the protrusion and retraction forces. The cross-linked actin filaments grow at a constant rate a while both filaments and bundles depolarize with rates c and e, respectively, and di use inside the cell [14]. Furthermore, some of the filaments align parallel to each other and form actin bundles and we assume that preexisting actin bundles help this alignment of actin filaments, leading to a non-linear coupling term. The resulting dynamical equations for V and W can be coupled to the phase field in a consistent way [9]:

$$\begin{aligned}\frac{\partial(\phi V)}{\partial t} &= \phi\left(a - bVW^2 - cV\right) + D_V \nabla\cdot(\phi\nabla V) \\ \frac{\partial(\phi W)}{\partial t} &= \phi\left(bVW^2 - eW\right) + D_W \nabla\cdot(\phi\nabla W)\end{aligned}$$

Note that the inclusion of these forces extends work by others [16–18,20] who focused on vesicles. Our model does not include, however, a coupling to the dynamics of the surrounding fluid as in recent work by Misbah and collaborators [17].

When keratocytes slide over the substrate, the adhesiveness between the cells and substrate, along with the attachment and detachment of cells from the substrate can be viewed as an e ective friction that is proportional to the local speed [32]: $F_{\text{fr}} = -\tau v$. At quasi-steady state (neglecting inertia), the total force is approximately zero ($F_{tot} = F_{ten}+F_{bend}+F_{area}+F_{prot}+F_{retr}+F_{fr} = 0$) and since the evolution of phase field φ follows $\frac{\partial\phi}{\partial t} = -\mathbf{v}\cdot\nabla\phi$. $\Delta\varphi$, we get the final equation for φ:

$$\tau \frac{\partial \phi}{\partial t} = -\kappa \left(\nabla^2 - \frac{G''}{\epsilon^2} \right) \left(\nabla^2 \phi - \frac{G'}{\epsilon^2} \right) + \gamma \left(\nabla^2 \phi - \frac{G'}{\epsilon^2} \right)$$
$$- M_A \left(\int \phi d\mathbf{r} - A_0 \right) |\nabla \phi| + (\alpha V - \beta W) |\nabla \phi|$$

Physically, this means that the friction force on the cell is balanced by the active protrusion and retraction forces, which are transmitted from the substrate onto the cell via adhesion complexes [11]. Thus, the total force from the substrate onto the cell vanishes, as can be explicitly checked for our computed solutions. In our model, as in real locomoting objects, the action of the active elements are not merely internal, but instead are coupled to the external surroundings (here the substrate) and can cause non-zero momentum transfer.

This fourth order nonlinear partial differential equation was solved using an alternating direction implicit scheme and a second order backward differentiation formula. We used a 600×200 rectangular grid with grid size of $0.1 \ \mu m$ and time step of $\Delta t = 10^{-4} s$. To cut the computing time, we move the computational box with the cell's centroid such that the boundary of this box is at least 25 grids points away from the cell membrane. We have verified that taking a larger computational box does not change the quantitative results. To further reduce the computational costs, we have parallelized the algorithm and the final code required approximately 4 hours on 4 CPUs for 200 s, which was long enough to reach a steady state.

Our two-dimensional simulation parameters are obtained from measured three dimensional values by assuming a cell height of $0.1 \ \mu m$. For example, the surface tension parameter in the simulations is derived from the measured value γ_{exp} by the conversion $\gamma = 0.1 \ \mu m \cdot \gamma_{exp}$. Experimental values for this parameter and for the bending rigidity are, to our knowledge, not available for keratocytes and we have taken values reported by shear flow experiments using *Dictyostelium* cells [24]: $\gamma_{exp} \sim 10 pN/\mu m$ and $\kappa_{exp} \sim 10 pN \mu m$. Note that the surface tension value is much lower than the values reported using micropipette aspiration [25,26] and that this discrepancy has been attributed to the role of the cytoskeleton [27]. Indeed, results obtained [28] using micropipette aspiration for cells in which actin polymerization has been abolished give values that are close to the one reported in Ref. [24]. Other values of the simulation parameters can be found in Table 1 and it is important to note that we can obtain similar qualitative results for a wide range of parameters.

A typical simulation started with a circular stationary cell with radius $r_0 = 4.0 \mu m$, V=1.1 and W=0 uniformly. Since our reaction-diffusion system is linearly stable, we break the symmetry by assigning a spatially varying concentration field for W. For example, we can take $W = W_0 y$ for $y < 0$ and $W = 0$ otherwise, where y is a randomly chosen direction and y=0 is at the cell's center. Simulations show that different asymmetric initial conditions lead to the same steady state. Due to the asymmetric distribution of W, the cell will retract from the edge with highest W and will start to move. As the cell moves forward, actin bundles are sequestered at the rear and its concentration is increased through the positive feedback loop while the cell's leading edge is characterized by a high concentration of cross linked actin filaments. A final steady state is reached when the cell has a stationary shape with a constant speed and stationary distributions of V and W. An example is shown in Fig. 1A for the particular set of parameter values of Table 1. The cell's area changed by less than 0.1% throughout the process. Fig. 1B and C show the steady state distribution of V and W.

To obtain different cell shapes and speeds we changed the value of growth rate a. The different cell shapes can be quantified by the aspect ratio S, defined as the ratio of the cell width and the cell length. When the growth rate a is small, the amount of V and W is limited

and the cell has little asymmetry. Therefore, the cell is nearly circular and moves slowly. Increasing the value of *a* corresponds to increasing the amount of both filaments network and bundle, providing larger driving forces for cell movement, and hence increases the cell's speed and aspect ratio. In Fig. 2A-C we plot the steady state solution of several cells with increasing speeds and aspect ratios.

Due to the coupling between the *V* and *W* field and the corresponding protrusion and retraction forces, there is a monotone relationship between the aspect ratio and the speed of the cell: the cell moves faster for larger aspect ratios. This is shown in Fig. 2D where we plot the speed as a function of the aspect ratio in our simulations (solid line). The cells shown in Fig. 2A-C correspond to the circles. As a comparison, we have also plotted the experimental results (dots) and the prediction of a simple model (dashed line) from Ref. [12]. This simple model does not compute the actual cell shape or the cell dynamics and determines the cell's speed based solely on the actin distribution. This is in contrast to our model, which explicitly provides the shape of the cell and requires a retraction mechanism, provided here by the *W* field. Furthermore, our simulation results, unlike the simple model, predict a zero velocity for $S = 1$. This corresponds to the case where the cross linked actin filaments and bundles concentration is distributed uniformly in the cell. Thus, there is no asymmetry and the cell will not move. To fit the results of our method we simply varied the friction coe cient and found that the value of τ given in the table gave the best fit to the experimental data. Clearly, the experimental data exhibits a large amount of variability, precluding a comparative quantitative analysis of the fits provided by the two models. Further progress would therefore depend on reducing this variability (if possible) by more tight protocols or on extending the model to allow for some degree of cell-to-cell parameter variability.

In summary, we have presented a phase field description of motile cell shapes. This method has a main advantage that it is able to find cell shapes without the need for an explicit boundary tracking algorithm. We find that, when applied to keratocyte motion, our model can obtain steady state cell shapes that agree qualitatively with experimentally observed shapes. Furthermore, we show that a simple change in parameters allows us to find a range of shapes with di erent aspect ratios and that the relationship between the resulting speed and aspect ratio agrees reasonably well with the experiments. The development of this method puts us in an excellent position to start addressing the coupling between intracellular dynamics and cell motion. A framework of the type proposed here is a necessary prerequisite for this future investigation. Finally, we are currently investigating the application of our ideas to other cell types in general, and chemotaxing cells in particular. There, the cells receive external signals that are translated into internal chemical cues [29,30]. Formulating models in which these internal cues generate significant cell deformations has been proved to be challenging [31]. Indeed, the coupling of models describing the internal pathways with cell motion is a difficult task, but one for which our method should be well suited.

Acknowledgments

References

[1]. Mogilner A. J Math Biol 2009;58:105. [PubMed: 18461331]

[2]. Janetopoulos C, Firtel RA. FEBS Lett 2008;582:2075. [PubMed: 18452713]

[3]. Alamo JCD, et al. Proc Natl Acad Sci U S A 2007;104:13343. [PubMed: 17684097]

[4]. Collins JB, Levine H. Phys. Rev. B 1985;31:6119.

[5]. Langer, J. Directions in condensed matter physics. World Scientific; Singapore: 1986. p. 1651986

[6]. Karma A, Rappel W-J. Phys. Rev. E 1998;57:4323.

[7]. Karma A, Kessler DA, Levine H. Phys Rev Lett 2001;87:045501. [PubMed: 11461627]

[8]. Folch R, et al. Phys Rev E 1999;60:1724.

[9]. Kockelkoren J, Levine H, Rappel WJ. Phys Rev E 2003;68:037702.

[10]. Fenton FH, et al. Chaos 2005;15:013502.

[11]. Fournier MF, et al. J. Cell Biol 2010;188:287. [PubMed: 20100912]

[12]. Keren K, et al. Nature 2008;453:475. [PubMed: 18497816]

[13]. Euteneuer U, Schliwa M. Nature 1984;310:58. [PubMed: 6377086]

[14]. Verkhovsky AB, Svitkina TM, Borisy GG. Curr Biol 1999;9:11. [PubMed: 9889119]

[15]. Lee J, et al. Nature 1993;362:167. [PubMed: 8450887]

[16]. Lowengrub JS, Ratz A, Voigt A. Phys Rev E Stat Nonlin Soft Matter Phys 2009;79:031926. [PubMed: 19391990]

[17]. Biben T, Kassner K, Misbah C. Phys Rev E 2005;72:041921.

[18]. Du Q, Liu C, Wang X. J Comp Phys 2006;212:757.

[19]. Biben T, Misbah C. Phys Rev E 2003;67:031908.

[20]. Campelo F, Hernndez-Machado A. Eur Phys J E 2006;20:37. [PubMed: 16733637]

[21]. Helfrich W. Z Naturforsch C 1973;28:693. [PubMed: 4273690]

[22]. Lecuit T, Lenne PF. Nat Rev Mol Cell Biol 2007;8:633. [PubMed: 17643125]

[23]. Mogilner A, Oster G. Curr Biol 2003;13:R721. [PubMed: 13678614]

[24]. Simson R, et al. Biophys J 1998;74:514. [PubMed: 9449351]

[25]. Dai J, et al. Biophys J 1999;77:1168. [PubMed: 10423462]

[26]. Reichl EM, et al. Curr Biol 2008;18:471. [PubMed: 18372178]

[27]. Merkel R, et al. Biophys J 2000;79:707. [PubMed: 10920005]

[28]. Zhang W, Robinson DN. Proc Natl Acad Sci U S A 2005;102:7186. [PubMed: 15870188]

[29]. Kutscher B, Devreotes P, Iglesias PA. Sci STKE 2004;2004

[30]. Levine H, Kessler DA, Rappel WJ. Proc Natl Acad Sci USA 2006;103:9761. [PubMed: 16782813]

[31]. Yang, L., et al. 2008. p. 68

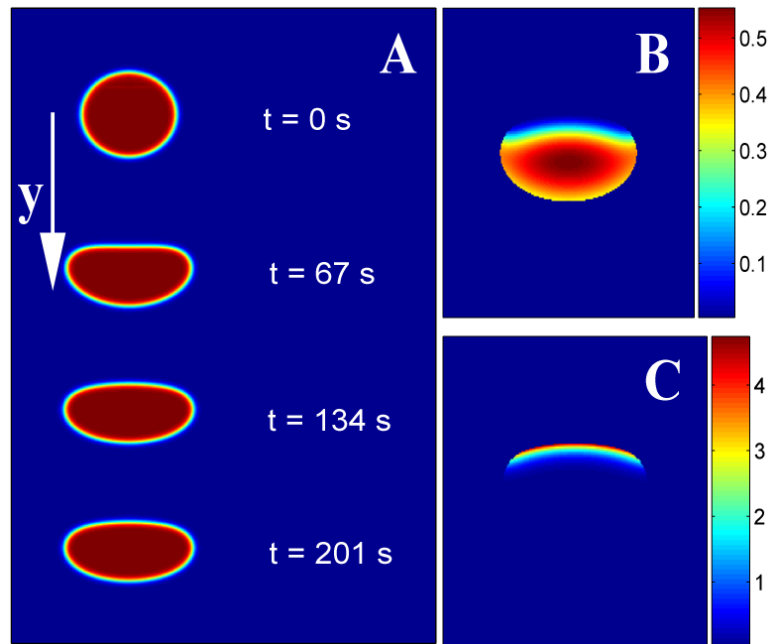[32]. Larripa K, Mogilner A. Physica A 2006;372:113. [PubMed: 19079754]

FIG. 1.
(Color online) A: Snapshots of the numerical evolution of a cell shape. The phase field is shown in a color scale with the interior of the cell ($\varphi = 1$) plotted as red and the exterior of the cell ($\varphi = 0$) plotted in blue. The resulting distributions of V and W are shown in B and C, respectively.
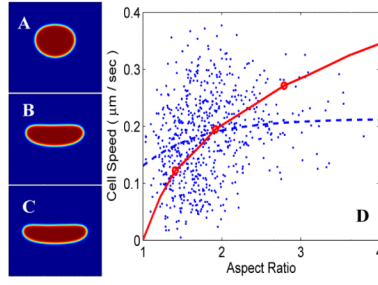
FIG. 2.
(Color online) Snapshots of three steady state solutions of our model for $a = 0.069s^{-1}$ (A), $a = 0.084s^{-1}$ (B) and $a = 0.107s^{-1}$ (C). The corresponding aspect ratios and cell speeds are $S = 1.41$ and $v = 0.12\mu m/s$, $S = 1.92$ and $v = 0.19\mu m/s$, and $S = 2.79$ and $v = 0.27\mu m/s$. D: Cell speed as a function of the aspect ratio. The solid line is our simulation result, the dots are experimental results from [12] and the dashed curve is the prediction from the simple model in [12]. The three circles correspond to A, B, and C.

TABLE I

Model Parameters

	Description	Value
γ	surface tension	1.0 pN
κ	bending rigidity	1.0 pNμm^2
α	coefficient of F-actin extension	0.1 $pN/\mu m$
β	coefficient of myosinII retraction	0.2 $pN/\mu m$
M_A	area constraint	1.0 $pN/\mu m^3$
A_0	prescribed area	50.24 μm^2
ε	3 times boundary width	1.0 μm
τ	friction coefficient	2.62 $pNs/\mu m^2$
a	actin filament growth rate	$0.084 s^{-1}$
b	actin filaments transform to bundles	$1.146 s^{-1}$
c	filament depolarization rate	$0.0764 s^{-1}$
e	bundle depolarization rate	$0.107 s^{-1}$
D_V	diffusion coefficient of actin filaments	$0.382 \mu m^2/s$
D_W	diffusion coefficient of actin bundles	$0.0764 \mu m^2/s$